small methods
www.small-methods.com

# Expansion and Light-Sheet Microscopy for Nanoscale 3D Imaging

*Luca Pesce,* Pietro Ricci, Giancarlo Sportelli, Nicola Belcari, and Giuseppe Sancataldo**

**Expansion Microscopy (ExM) and Light-Sheet Fluorescence Microscopy (LSFM) are forefront imaging techniques that enable high-resolution visualization of biological specimens. ExM enhances nanoscale investigation using conventional fluorescence microscopes, while LSFM offers rapid, minimally invasive imaging over large volumes. This review explores the joint advancements of ExM and LSFM, focusing on the excellent performance of the integrated modality obtained from the combination of the two, which is refer to as ExLSFM. In doing so, the chemical processes required for ExM, the tailored optical setup of LSFM for examining expanded samples, and the adjustments in sample preparation for accurate data collection are emphasized. It is delve into various specimen types studied using this integrated method and assess its potential for future applications. The goal of this literature review is to enrich the comprehension of ExM and LSFM, encouraging their wider use and ongoing development, looking forward to the upcoming challenges, and anticipating innovations in these imaging techniques.**

## 1. Introduction

For centuries, optical microscopy has contributed to scientific research, enabling us to explore the intricate details of life at the cellular and molecular levels.[1] In recent years, two innovative microscopy techniques, Expansion Microscopy (ExM) and Light-Sheet Fluorescence Microscopy (LSFM), have emerged as groundbreaking approaches that revolutionize our ability to visualize and understand biological structures with enhanced clarity and depth.

ExM is a recent technique that overcomes the traditional limitations of optical microscopy. Previously, the physics-imposed diffraction limits the spatial resolution to a few hundred nanometers, notably larger than individual biological molecules.[2] Rather than trying to improve the imaging system's performance to capture finer details,[3,4] ExM introduces an opposite approach: physically enlarging biological specimens. The process involves embedding the sample in a swellable hydrogel matrix and then expanding it by adding water. This expansion effectively separates molecules that were initially too close to be resolved by traditional microscopy, allowing for nanoscopic super-resolution imaging without the need for specialized equipment. ExM offers a transformative solution to the longstanding resolution limit imposed by the diffraction of light.[5] By physically expanding the sample, structures that were once blurred together can now be distinguished and studied in detail. This technique has profound implications for studying intricate cellular structures, protein interactions, and spatial relationships within biological samples. The capacity to finely adjust the expansion factor (from 4× to 20× linear expansion factor,[2] EF), thereby enhancing optical resolution, alongside the concurrent reduction in the refractive index of specimens – features shared with established clearing methodologies[6] – creates a synergistic effect, in particular when combined with opportune optical setup.

LSFM, also known as selective plane illumination microscopy (SPIM), represents another paradigm shift in imaging techniques. Born out of the need to mitigate phototoxicity and improve imaging speed with respect to other classical scanning methods, LSFM utilizes a fundamentally different, faster, and gentler approach to illuminate the sample. Instead of illuminating the entire specimen, as in traditional widefield microscopy, a thin sheet of light is used to illuminate and then visualize a specific plane of interest within the sample. This innovative approach drastically reduces light exposure and minimizes damage to the specimen, enabling researchers to capture dynamic processes and delicate structures with minimal perturbation. Moreover, LSFM's optical sectioning capabilities yield fast, 3D images, making it a preferred choice for studying complex biological systems. This technique has provided previously unattain-

L. Pesce, G. Sportelli, N. Belcari
Department of Physics – Enrico Fermi
University of Pisa
Largo Pontecorvo, 3, Pisa 56127, Italy
E-mail: luca.pesce@unipi.it
P. Ricci
Department of Applied Physics
University of Barcelona
C/Martí i Franquès, 1, Barcelona 08028, Spain
G. Sancataldo
Department of Physics – Emilio Segrè
University of Palermo
Viale delle Scienze, 18, Palermo 90128, Italy
E-mail: giuseppe.sancataldo@unipa.it

The ORCID identification number(s) for the author(s) of this article can be found under https://doi.org/10.1002/smtd.202301715



**DOI: 10.1002/smtd.202301715**

able insights with conventional microscopy methods, from observing embryonic development to tracking cellular dynamics and imaging large cleared samples.[6] In addition, the combination of LSFM and ExM yields benefits. Indeed, the optical resolution of LSFM is confined by the diffraction limit as defined by the Abbe law.[5] To overcome this constraint, an effective strategy involves integrating LSFM with ExM, thereby "transforming" LSFM into a powerful super-resolution approach. On the other side, ExM was initially devised as a super-resolution technique integrated with conventional diffracted microscopes (i.e., confocal and widefield microscopes).[7] While these methodologies excel in multicolor nanoscale imaging of biological specimens, they are limited in their capacity for volumetric reconstruction. Using conventional optical systems, the reconstruction of expanded samples can be time-consuming, although improved approaches, like a spinning disk confocal microscope,[8] may be considered for spatial mapping. Further considerations need to be taken into account regarding the combined approach of ExM and super-resolution optical instruments (i.e., ExSTED,[9–11] ExSTORM,[12,13] and ExSIM[14]). Although these approaches are limited to a few fluorophores and require a specific oxygen-scavenging buffer system, recent works have demonstrated the capability of imaging expanded samples with a spatial optical resolution down to 20 nm.[9,10,12] Nevertheless, the methodologies outlined previously lack a crucial aspect when it comes to examining intricate biological samples: the capability to explore the sample within its nanoscale context, considering the interactions and features of the sample as a cohesive entity. Indeed, these methods lose effectiveness when examining tissue samples or organs, thus giving up the opportunity to study the specimens as a whole. In combination, ExM and LSFM referred to as ExLSFM, offer complementary strengths that amplify each other's capabilities. The rapid and gentle acquisition rate of LSFM aligns seamlessly with cleared and expanded tissues. Specifically, ExLSFM exhibits compatibility with diverse sample types and expansion factors, does not require a specific buffer and antibody-conjugated fluorophore for imaging, and enables comprehensive visualization of specimens in all their intricacies. This review explores the principles, applications, and transformative impact of ExLSFM. We show how these techniques have paved the way to probe intricate biological systems, from cells to whole-expanded organs. By examining their technological advancements, from optical configurations to ExM protocols, and considering the diverse biological samples they have targeted, we emphasize the significant potential their integrated approach offers for future applications.

## 2. Expansion Microscopy

### 2.1. Procedure Overview

The primary goal of expanding biological specimens is to uniformly magnify them in all 3D using optical fluorescence microscopy (**Figure 1a**).[2] Over recent years, various labeling strategies have been developed, and these can be used to categorize the ExM procedure. These include i) pre-expansion labeling, ii) expressing fluorescent proteins or self-labeling proteins, and iii) postexpansion labeling.[2,15] Fluorescent labels can be applied to targeted biomolecules either before the formation of the hydrogel, which is specific to ExM, or following gelation, which is what we call post-expansion and is usually referred to as Magnified Analysis of the Proteome (MAP).[16] For a clear and effective ExM procedure, there are five primary steps commonly adopted across various methodologies. However, the order of preparation in these steps may vary (Figure 1b). Briefly, we outline the main steps in the conventional ExM approach (Pre-expansion labeling), which can be divided into:

1) Staining: the sample is fixed to preserve and stain it with specific fluorescent probes (see "Section 2.1.1 Preserving biological integrity: an overview of tissue fixation techniques and chemical agents");
2) Anchoring: the specimen is modified using chemical anchors. These anchors are employed to retain the labels within the hydrogel (see "Section 2.1.2 State of the art of biomolecular anchoring techniques");
3) Gelation: the specimen is incubated into a swellable hydrogel. Different compositions and hydrogel recipes have been developed according to the achievable sample characteristics and expansion factor (see "2.1.3 Hydrogel formation and signal retention of fluorescent dyes");
4) Homogenization: the hybrid hydrogel/sample is typically accomplished through enzyme digestion or heat denaturation to disrupt the interactions among biomolecules (see "Section 2.1.4 Homogenization");
5) Expansion: the electrolytes present in the swellable hydrogel facilitate water absorption and subsequent expansion of the specimen (see "Section 2.1.5 Expansion").

Each stage of the ExM protocol and its variants will be detailed, emphasizing sample preparation for tissues and organs and precautions for acquisition using LSFM.

#### *2.1.1. Preserving Biological Integrity: Tissue Fixation Techniques and Chemical Agents*

Fixatives serve multiple purposes. Primarily, they protect tissues from autolysis (caused by enzymes) and putrefaction (due to bacteria). Moreover, fixatives preserve the relationship between cells and external compartments by rendering them nonsoluble, minimizing alterations from subsequent processes, and preventing osmotic harm that might lead to tissue contraction or expansion.[17] The most common method of chemically fixing biological specimens involves using paraformaldehyde (PFA) to cross-link primary amines in proteins. PFA interacts with nucleic acids and proteins, forming stable nucleic acid-protein complexes,[17,18] forming highly reactive methylol compounds upon interaction with amine groups present in endogenous biomolecules. Alternatively, fixatives such as glutaraldehyde (GA) can enhance structural preservation, despite its low penetration rate into the samples.[17] GA has two aldehyde groups linked by a flexible chain of three carbon atoms, which allows it to induce greater protein cross-linking and structural preservation compared to PFA. Combinations of PFA and GA lead to precise fixation and decrease the movement of molecules, likely due to enhanced protein cross-linking.[19] For animals (such as mice), transcardial perfusion with PFA in PBS, or a combination of PFA and GA, is generally performed to flush out the blood from the circulatory system and efficiently reach all parts of the brain and

 

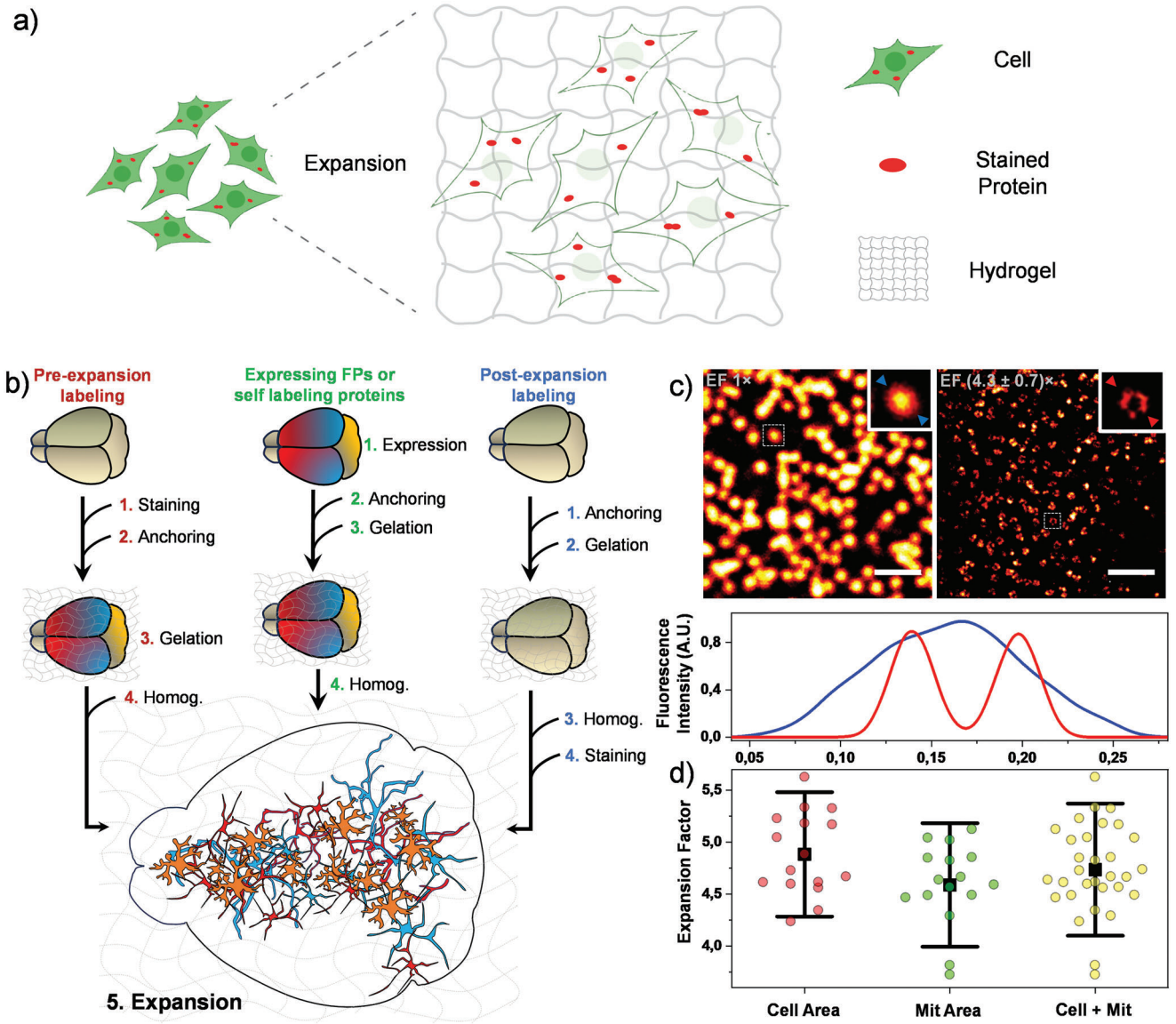


**Figure 1.** ExM protocols, optical resolution improvement, and expansion factor (EF) estimation. a) Schematic representation of the expansion process. b) Three distinct labelling methods in ExM. The representation of a section of a mouse brain to depict the various stages associated with each ExM method used (homog. corresponds to homogenization). c) Resolution enhancement demonstrated using the Nuclear Pore Complex (NPC). Confocal images depict NPCs stained for Nup153, both pre (Expansion Factor, EF = 1×) and postexpansion (EF = (4.3 ± 0.7)×), alongside their respective intensity plot profiles. Scale bar pre-expansion: 1 µm; scale bar postexpansion: 4 µm/4 = 1 µm. d) Characterization of the EF using both subcellular (mitochondria) and cellular (actin staining) markers. The determined EF for mitochondria and cell area is 4.7 ± 0.43 (SD). Due to variations in expansion rates among cellular regions, relying solely on the average expansion of one feature may lead to inaccuracies. It's recommended to assess EFs across various biological features for more precise EF determination. The experimental values are based on a total of 30 cells, with 15 cells each for actin staining and mitochondria analysis. Panels c and d were adapted with permission from refs. [9,52].

body. In some methods, a hydrogel solution is used during perfusion to enhance structural preservation and facilitate subsequent embedding in a hydrogel mesh[16,20] (referred to "*hydrogel formation*"). Also, fixatives like glyoxal and cryo-fixation enhance antigenicity and achieve superior structural preservation. Notably, glyoxal is a dialdehyde with two carbon atoms, and its aldehyde groups are highly reactive.[17] Studies have shown that samples preserved with glyoxal exhibit high cellular preservation, making it ideal for super-resolution imaging.[21] It should be noted that the choice of fixative can influence the final signal-to-noise ratio. For instance, GA can result in elevated background fluorescence,[22] which may impact the quality of the expanded sample acquisition.

However, methods that utilize these strategies inherently face a significant limitation arising from covalent crosslinking: the chemical alteration of biomolecules. Many endogenous proteins present amine-rich amino acids on their exteriors (i.e., lysine and arginine), susceptible to reactions with fixatives. As mentioned

 

earlier, this chemical alteration is vital for maintaining the tissue's structure. However, modifying these surface residues could lead to damage to the epitope. Indeed, during the hydrogel polymerization in ExM, elongated acrylic polymer chains, whether attached directly to methylol-carrying epitopes or close, may obstruct antibody-epitope interactions (referred to postexpansion labeling method). The repercussions of this covalent integration between tissue and hydrogel manifest as a loss in epitope diversity, significantly narrowing the range of commercially accessible antibodies suitable for probing biological systems. In 2021, Chung and team[23] effectively tackled this major limitation in the study of biological materials using expansion protocols. Their method begins with perfusion using PFA, devoid of the gel mixture, followed by a rinsing step to eliminate surplus formaldehyde before gel formation. During this thorough rinse, the uncombined methylols may revert to formaldehyde due to the reversible nature of the methylol formation, thereby reinstating the native characteristics of the associated amino acids. Subsequently, the tissue is immersed in a hydrogel monomer solution composed of a high concentration of acrylamide. The hydrogel monomer solution is devoid of formaldehyde, ensuring that acrylic monomers remain inert toward endogenous biomolecules. Consequently, these biomolecules aren't covalently attached to the expandable gel matrix but are physically entrapped. While fixative molecules have played an essential role in studying biological specimens, their chemical modifications can sometimes obscure accurate analysis. Thus, specific ExM variants have been developed to address this challenge, enabling a more precise examination of biomolecules' native organization at the nanoscale.

### 2.1.2. State of the Art of Biomolecular Anchoring Techniques

The novelty of the sample expansion protocols is the introduction of small anchors that act as a bridge between the sample and the hydrogel. These small molecules are inserted immediately after the fixation and, eventually, permeabilization of the sample. The anchoring of biomolecules can be achieved either by directly preserving the biomolecule itself or by maintaining the affinity probes used to stain specific biological features. Historically, the first approach used affinity probes, predominantly antibodies conjugated to DNA oligonucleotides, called trifunctional labels, explicitly made for ExM.[7] These labels can bind to the target molecule through bioconjugation, become part of the hydrogel structure, and provide a fluorescent readout due to an incorporated fluorophore. The primary focus of this technique was to study proteins. The tri-functional probe has 1) a methacryloyl component that can be incorporated in the mesh gel during the polymerization, 2) a fluorescent molecule for imaging purposes, and 3) an oligonucleotide strand that can bind to a matching sequence linked to an affinity label, e.g., a secondary antibody.[7] Affinity probes had inherent complexities, though. Notably, custom-conjugated antibodies to DNA oligonucleotides were required, which were not commercially available. As a result, ExM was not widely adopted in its initial form. Introducing bivalent chemical linkers, namely acryloyl-X (AcX)[22] and methacrylic N-hydroxysuccinimide (MA-NHS),[24] solved this issue. AcX and MA-NHS work as crosslinkers that form covalent bonds between the target biomolecules and the hydrogel. For example, MA-NHS reacts with the primary amines of proteins using its NHS ester group, while its methacrylamide group integrates into the polyacrylic chains of the hydrogel. An alternative method involves cross-linking gel polymers and proteins using GA. However, the exact way glutaraldehyde-treated samples link proteins to hydrogel is unclear. In water, glutaraldehyde exists as a mixture, shifting between monomeric and polymeric forms, each having aldehyde and alkene components. Both these components could theoretically be incorporated into the acrylamide polymer.[24] Traditionally, the initial methods developed in this domain were primarily focused on targeting proteins within biological specimens. Recognizing this limitation and the need for more versatile techniques, Boyden and colleagues introduced the ExFISH method. ExFISH utilizes an anchor named LabelX. This anchor possesses an alkylating group for labeling guanine in RNA and an acrylamide group for crosslinking to the hydrogel.[25] One notable advantage of this method is the simultaneous visualization of endogenous YFP protein, which is anchored to the polyacrylate gel via AcX, and RNA which is anchored via LabelX.

Soon after, new ExM methods were introduced that enabled both the preservation and examination of native proteins following homogenization. The pioneering postexpansion labelling method is MAP (Magnified Analysis of the Proteome),[16] and then its evolution, termed eMAP (Epitope-preserving magnified analysis of proteome).[23] This method was later adopted in other techniques, such as ZOOM[20] and MAGNIFY.[26] Also, proExM,[22] which exploits the anchor AcX, can retain the endogenous biomolecules and perform postexpansion labeling. The MAP technique, developed concurrently but independently from proExM, also supports preserving and labeling epitopes postexpansion. However, its fixation, polymerization, and homogenization processes differ slightly. In the MAP approach, the spacing between proteins embedded in the gel increases by reducing cross-linking between proteins during the formaldehyde fixation phase. This reduction is achieved by introducing acrylamide during the fixation process. The acrylamide interacts with the formaldehyde bound to proteins, thus inhibiting protein-to-protein cross-linking.[16] The MAP protocol has also been combined with SHIELD (Stabilization under Harsh conditions via Intramolecular Epoxide Linkages to prevent Degradation) to simultaneously preserve biological information, including protein fluorescence, protein immunoreactivity, and nucleic acids in cleared intact tissues.[27] In recent years, significant research activity has been focused on discovering new anchoring molecules that are universal for various types of biomolecules. This enables simultaneous nanoscale multiplexed imaging of various biomolecules, leading to more precise probing of biological samples. Indeed, researchers have formulated universal anchoring strategies applicable to various biomolecules and not restricted to proteins, including nucleic acids and lipids, potentially increasing the versatility of ExM (for example, MAGNIFY[26]).

### 2.1.3. Hydrogel Formation and Signal Retention of Fluorescent Dyes

The anchoring procedure is essential for preserving the accurate 3D arrangement of biomolecules in the specimens. Similarly, achieving a dense and uniform hydrogel is crucial for

the proper visualization of these biomolecules. The foundational hydrogel composition is derived from a monomer mixture combining nonionic acrylamide and ionic acrylate. N'N'-methylenebisacrylamide is introduced as a crosslinking agent to link these polymer chains together. The gel solution is further enriched with ammonium persulfate (APS) or potassium persulfate, an initiator, to instigate free-radical polymerization.[15,28] To accelerate this process, tetramethylethylenediamine (TEMED) is integrated into the mixture. The cascade can also be initiated using heat-responsive initiators like VA-044 or V-50, or the light-responsive initiator, riboflavin 5′-monophosphate.[28] The use of APS/TEMED produced significant auto-fluorescent background, particularly noticeable in ExFISH where signals are inherently faint.[25,29] In contrast, VA-044 is preferred because it produces minimal auto-fluorescence, making it ideal for ExFISH.[29] Additionally, VA-044 is particularly well-suited for tissues and whole organs. At low temperatures (4 °C), it allows gelling reagents to diffuse thoroughly into the thick samples' core; then, at elevated temperatures (37 °C), it promotes a homogeneous polymerization.[16,30] Notably, the properties of the gel composition are inextricably linked to the achievable expansion factor. For instance, increasing the monomer concentration is a recognized strategy for refining the expansion coefficient, as showcased by the ×10-ExM protocol,[31,32] which enables a tenfold expansion of the specimen. On the other hand, decreasing the concentration of crosslinkers – thereby enhancing gel elasticity – positively influences the expansion coefficient. This relationship is further evidenced by the ten-fold robust expansion microscopy (TREx),[33] capable of producing sample expansions from four-fold to 14-fold. For a comprehensive examination of existing gels, we recommend the review conducted by Truckenbrodt.[28]

In most ExM variations, the inevitable degradation of dyes occurs through free radical-induced processes during the polymerization step.[7,34] The highly reactive nature of the radical intermediates induces side reactions, resulting in the breakdown of dye scaffolds. This issue is pervasive among all organic dyes and can influence the post-expansion imaging of the sample. Notably, popular cyanine dyes like Cy3 and Cy5 are particularly susceptible, with almost destruction during the polymerization step in ExM.[35] Consequently, this significantly diminishes the fluorescent signal intensity post-expansion, limiting the achievable imaging quality in ExM. To address this drawback, two primary strategies can be employed. The first involves postexpansion labeling, extending to encompass the polymerization process. However, this methodology necessitates robust tissue preservation, and precautions should be taken to prevent epitope loss during homogenization.[16,23] The second approach involves the use of 4-nitrophenylalanine (NPA)-conjugated fluorophores, which exhibit increased retention of fluorescent signals during the free-radical polymerization process.[35] This improvement is attributed to the protection of dyes against radical-induced degradation and photoprotection during imaging.

#### 2.1.4. Homogenization: Fundamentals and Strategies

Consistent homogenization ensures that the hybrid sample/hydrogel expands uniformly. If there are differences in these properties, certain areas might not expand uniformly, which could cause distortion or weaken the structure. To achieve mechanical homogenization, it is necessary to destruct the complex biomolecular interactions that confer structural integrity to biological samples. Homogenization is predominantly realized through two strategic approaches in different expansion protocols: Enzymatic Proteolysis or Thermal-Chaotropic Denaturation.[28] Enzymatic Proteolysis employs enzymes to degrade pivotal biomolecules. Historically, such indiscriminate proteolytic enzymatic digestion was the technique of choice for expanding mammalian brain tissues and in vitro mammalian cell cultures.[7] Instead, in the Thermal-Chaotropic Denaturation process, protein–protein interactions are perturbed through the combined action of elevated temperatures and chaotropic agents. Respecting enzymatic proteolysis, this approach offers the added benefit of antigen preservation, which facilitates subsequent immunohistochemical analyses. Typically, the antibodies employed in traditional immunofluorescence protocols, such as IgG (with a size of 150 kDa and a length of 15 nm[36]), are bigger than the target proteins. This size discrepancy can complicate the labeling of tightly packed proteins. As a consequence, it becomes challenging to label densely packed proteins. For example, in the MAP protocol, a high acrylamide concentration in the gel composition reduces inter-protein crosslinking and generates a heat- and chemical-resistant hybrid tissue/gel.[16] The decrowding effect generated by denaturation at high temperatures improves antibody diffusion into the tissue and facilitates epitope recognition by antibodies after expansion. Recent new protocols and/or applications of ExM indicate a shift toward this last method, which requires a specific composition of the hydrogel and/or opportune anchor molecules.

#### 2.1.5. Expanding Hydrogels for Enhanced Imaging

Hydrogels in ExM are polymeric networks capable of absorbing significant quantities of water while maintaining their shape. Most of these hydrogels possess anionic side groups that are equilibrated with metal cations during both the polymerization phase and in their pre-expanded state. Eliminating these metal cations through serial distilled water rinses instigates electrostatic repulsion amongst the anionic moieties, culminating in the enlargement of the hydrogel-biological specimen hybrid. Given a thorough homogenization of the biological specimen, the composite experiences an isotropic expansion, conserving the relative spatial configuration of biomolecules whilst amplifying its overall volume[9,37] (Figure 1c). For example, sodium acrylate constitutes the primary backbone of the meshgel, which facilitates the formation of a swellable hydrogel. The positively charged sodium ions are removed upon rinsing with deionized water, leaving behind the negatively charged carboxyl groups on the polymer backbone. This results in electrostatic repulsion between these carboxyl groups, inducing a stretching force and subsequently causing the expansion of the polymer.[38]

### 2.2. Isotropic Expansion: Influential Factors and Solutions

Extracting insights from numerous scientific studies, it becomes evident that various factors influence the isotropy of the expansion process. These encompass intrinsic sample characteristics,

such as collagen density or prolonged fixation, extending to the preparation of the matrix gel. However, these influences can be mitigated through specific adjustments.

Anisotropic expansion commonly arises from the over-crosslinking of proteins during fixation. The choice of a suitable fixation method plays a crucial role in mitigating local distortions. Notably, Ultrastructure Expansion Microscopy (U-ExM)[39] has demonstrated near-native structural expansion of cellular contents by employing a gentle fixation approach, combining low formaldehyde and acrylamide incubation. Building on U-ExM, cryofixation ExM emerges as a method to preserve the native structural organization of cellular contents through rapid cryofixation.[40] It is imperative to consider paraffin-embedded samples, as they often undergo prolonged fixation and paraffin embedding, inducing anisotropic expansion due to inter- and intramolecular binding effects caused by formaldehyde and amino groups of proteins during extended fixation.[41] To counteract these effects, one can either process thin slices of pathological tissue combined with treatment with 20 mM sodium citrate at pH 8 and 100 °C[42] or employ high-temperature homogenization combined with a hydrogel recipe possessing robust mechanical characteristics.[23,43]

An essential factor contributing to isotropic expansion is the limited diffusion of monomers leading to premature gelation, particularly pronounced in thick samples and whole organs. To address this challenge, the addition of a surfactant (such as Triton X-100 or saponin) to both the AcX solution and hydrogel solution proves effective, enhancing the deep diffusion of these materials into the specimens. In the gelation process, substituting the traditional mixture of APS, TEMED, and 4-HT with the thermal initiator VA-044 offers a viable alternative.[16] This modification extends the sample's incubation time in the hydrogel solution to 24 h or more. In contrast, employing a hydrogel solution containing APS, TEMED, and 4-HT resulted in rapid gel formation within 1 h, even at 4 °C, which is compatible with cell culture[29] and small spheroids,[44] but it makes prolonged incubation unfeasible.

Incomplete sample homogenization stands out as a significant contributor to structural distortion. While enzymatic denaturation proves to be an effective method for sample homogenization, the drawback of utilizing proteinase K is the consequential signal loss, especially in high-density biological samples that necessitate prolonged digestion times. Opting for thermal denaturation can be the preferred choice, contingent upon efficient functionalization and the use of a dense mesh gel to preserve epitopes. Furthermore, the adoption of novel, less deformable hydrogel types can contribute to a more uniform expansion across the entire sample. Consideration should be given to a recent advancement involving the utilization of a highly homogeneous polymer made up of tetrahedron-like monomers.[45] This innovation has been reported to enhance isotropy in ExM methodologies significantly.

Finally, intrinsic sample characteristics play a pivotal role in the ExM process. Specifically, the presence of connective tissue in vertebrate organ slices and tumor specimens, which are characterized by mechanically resistant collagen, requires meticulous consideration during the homogenization process. Specific ExM protocols, particularly those with higher expansion factors such as ×10, face challenges when expanding these resistant samples.[31] To overcome this hurdle, some studies propose the use of collagenase treatment to achieve isotropic expansion, particularly in tissues like kidney specimens.[46] A promising alternative has emerged through a protease-free homogenization approach. This method involves autoclaving tissue in a buffer solution containing SDS and has recently been demonstrated for both ×4[22] and ×10[47] expansion factors. Notably, this approach significantly broadens applicability, even for thick tissue sections, by eliminating the need for collagenase treatment and expanding the potential of ExM in challenging sample scenarios. While bone has traditionally posed a significant challenge for ExM studies, recent work by Sim et al.[48] showcased successful expansion in the Zebrafish model. The optimized protocol, known as Whole-ExM,[48] incorporates repetitive proteinase digestion and treatment with the decalcifying agent ethylenediaminetetraacetic acid (EDTA), commonly used in histology and bone clearing for decalcification. Applying the decalcification process after digestion, this protocol achieved a remarkable 4.1-fold expansion in larvae aged 3–12 days postfertilization.

### 2.3. Resolution Estimation

The effective resolution of ExM, denoted as $R_{\text{eff}}$, is governed by two primary parameters: the inherent resolution of the microscope, $R_{\text{micro}}$, and the hydrogel's length expansion factor, $EF$. A higher value of $EF$ correlates with enhanced ExM resolution as:

$$R_{\text{eff}} = \frac{R_{\text{micro}}}{EF} \tag{1}$$

$R_{\text{micro}}$ can be determined, for example, using fluorescent beads. It depends on the numerical aperture of the objective lens and the wavelength, as outlined by Abbe's law. Several aspects can influence the magnitude of the EF, such as the osmotic pressure induced by polymer and biomolecule concentrations, the elasticity of the gel-sample hybrid system, the presence of mobile ions within this system, and the purity of the stock solution of sodium acrylate. For instance, the standard ExM and proExM techniques achieve approximately a 4.5× linear expansion,[7] while iExM[49] allows an expansion of approximately 4.5× or 20×. For an objective lens with a ≈300 nm diffraction limit, a 4.5× expansion protocol provides an effective resolution of roughly 60–70 nm. With a 20× expansion, the theoretical resolution would be ≈15 nm. However, for the iExM's documented approach, antibody size pre-expansion sets a resolution bottleneck, resulting in an actual resolution of 25 nm.[38,50] Thus, an accurate measure of the EF is crucial for predicting resolution outcomes, establishing accurate distances on the original biological scale, and interpreting data correctly. Various methods exist for calculating this factor, from the evaluation of the gel's physical dimensions (millimeter-scale) and weight before and after expansion to the measurement of typical cellular features, such as nuclei, pre and postexpansion. However, these methods are often less precise than imaging a sample section before expansion and then re-imaging that same section after expansion[9,51] (e.g., examining cellular components like mitochondria or nuclear pore complexes, Figure 1c). This latter method tends to produce the most consistent results.[52] As different cellular regions expand at varying rates,[9] relying

 

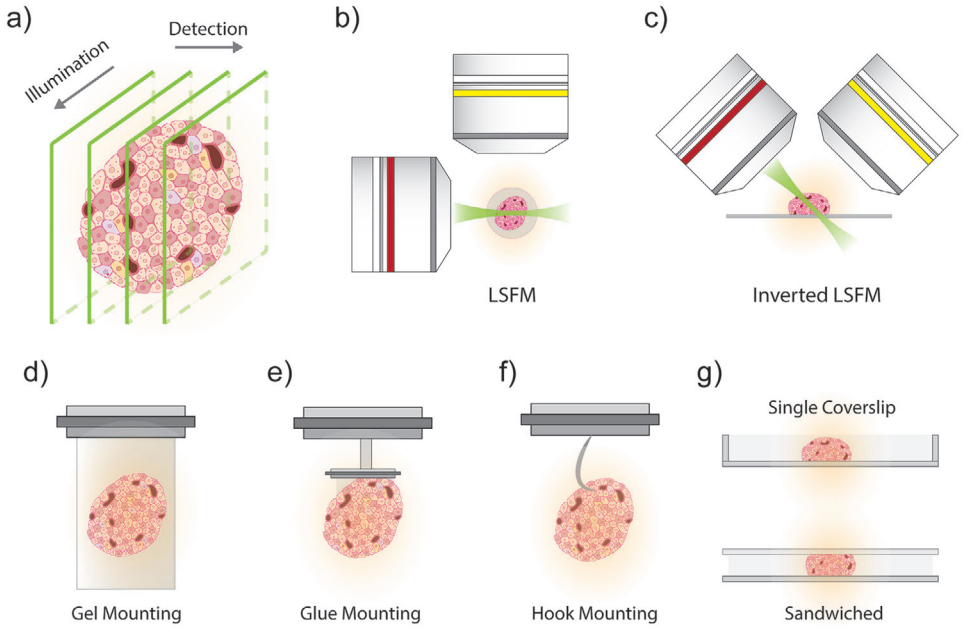


**Figure 2.** Light-Sheet Microscopy: optical setups and mounting strategies. a) Schematic of the plane-by-plane illumination of specimens in LSFM. b) Optical architectures of LSFM and c) inverted LSFM. d) Hydrogel sample mounting, e) glue mounting, and f) hook mounting. g) common mounting for inverted LSFM.

on the average expansion of a single cellular feature can introduce errors. Therefore, it's recommended to estimate the EF across a range of biological features (Figure 1d), which helps ascertain a more accurate EF. Misestimations of the EF can lead to significant inaccuracies, especially in nanoscale biological research.

Notably, the type of structure under examination and the labeling density significantly influence the reliability of the acquired information.[53] It is crucial that the labeling of the imaged structures is uniform and that the nearest-neighbor distance between fluorophores, within the structure of interest, is not larger than half the achievable resolution. This is especially important for ExM since, even if uniform and satisfactory dense labeling is achieved in the pre-expansion sample, the stretching process of the hydrogel during the expansion process can introduce "false" gaps. This can lead to the resulting image being highly resolved data with compromised interpretability. Finally, both the density of labeling and the nature of the structure being labeled emerge as pivotal factors influencing the outcome.

## 3. Light-Sheet Microscopy for the Imaging of 3D Samples

### 3.1. Fundamentals of Light-Sheet Microscopy

Advanced optical methods are essential for achieving fast volumetric imaging of biological specimens. Among these methods, LSFM has emerged as a pivotal platform that effectively addresses these objectives[54] and has proven its efficacy in imaging thick samples. The origins of the technique can be traced back to the early 20th century when it was first proposed as an imaging method (known as Ultramicroscope) by Richard Zsigmondy and Henry Siedentopf.[55] However, the technique remained largely underexplored until the years turning the century, when Spelman et al.[56] and Stelzer et al.[57] demonstrated its feasibility and potential in capturing 3D images of biological specimens and live samples. Since then, LSFM has undergone significant advancements in technology and methodology, making it an essential tool in contemporary biological research.[58,59]

Unlike traditional wide-field microscopes, where the sample is entirely illuminated, LSFM makes use of a thin sheet of light to selectively illuminate the specimen plane-by-plane (**Figure 2a**), while the fluorescent emission is collected along the orthogonal direction (Figure 2b). The sample is typically positioned in the overlap between the illumination and detection focus, such that a 2D image of the section is produced and recorded by a camera detector. Then, the observation volume is usually translated over the whole sample to acquire 3D image stacks and reconstruct the entire structure. Thanks to its capacity for rapid imaging across a broad field of view while maintaining sample integrity and delivering high-quality images, LSFM emerges as an exceptionally fitting choice for imaging expanded samples such as tissues, whole organs, and animals. In particular, LSFM is compatible with various model organisms, such as zebrafish,[60,61] Drosophila,[62] and C. elegans,[63] making it ideal for developmental biology,[64,65] neuroscience studies[65] and expanded samples. Indeed, due to the LSFM particular configuration, by illuminating only the focal plane of interest, the phototoxicity, and photobleaching of the remaining parts of the sample are effectively reduced.[66]

Moreover, since this geometry requires two distinguished objectives to be used, the lateral and axial optical resolution of the

 

system can be completely decoupled from each other. In detail, assuming for simplicity a Gaussian beam illumination, they can be described as:[67]

$$R_{\text{lateral}} = \frac{0.61 \times \lambda_{\text{em}}}{NA_{\text{det}}} \tag{2}$$

$$R_{axial} = \frac{2 \times \lambda_{\text{ex}}}{\pi \times NA_{\text{ill}}} \tag{3}$$

where $\lambda_{\text{em}}$ and $\lambda_{\text{ex}}$ are the emission and excitation wavelength, respectively; and $NA_{\text{det}}$ and $NA_{\text{ill}}$ are the numerical aperture of the detection objective and illumination objective, respectively. Notably, Equation (3) also defines the thickness of the sheet of light used to illuminate the sample, which often is dominant in the axial resolution evaluation. In the end, also the field of view of illumination ($FOV_{\text{ill}}$) is related to these previous parameters. Specifically, $FOV_{\text{ill}}$ is the region where the illumination intensity can be considered uniform for the sample, and only depends on the characteristics of the excitation beam and of the illumination objective, as:[68]

$$FOV_{\text{ill}} = \frac{1.78 \times n \times \lambda_{\text{ex}}}{NA_{\text{ill}}^2} \tag{4}$$

Therefore, depending on the sample geometry, objectives with different $NA_{\text{det}}$ and $NA_{\text{ill}}$ are often used, with optimized resolutions and depths of field.[69]

### 3.2. Optical Schemes of Light-Sheet Microscopy

The success of LSFM hinges on the design and construction of specialized imaging systems. A typical LSFM setup consists of two perpendicular optical paths: one for illumination and the other for detection. The illumination path employs a light sheet generator such as a cylindrical lens[57,70] or a rapid scanner for the beam (digitally scanned laser light-sheet fluorescence microscopy – DSLM).[64,71] To improve image quality and fulfill specific specimen characteristics, several illumination approaches alternative to the Gaussian beams have been adopted over time, spanning from the Airy beam[72] to the Bessel beam.[73,74] On the detection side, standard setups usually comprise high-sensitivity cameras capable of capturing fluorescence signals emitted by the illuminated sample. Notably, several efforts have been spent to increase the image contrast, for example, by exploiting the confocal detection of the emitted signal.[75,76]

In the last decades, a large variety of optical architectures have been proposed. Single-sided illumination (also widely known as Single-plane Illumination Microscopy) is one of the earliest and simplest optical schemes used in LSFM (Figure 2b). This approach involves the illumination of a specimen from one side while capturing the fluorescence signal from the orthogonal direction. Despite the low photodamage and the high precision allowed, single-sided imaging of thick samples can lead to shadowing artifacts,[77] limited imaging depth, and significant differences in image quality within the same field of view. To address these shortcomings, multi-directional illumination[71,78,79] has been developed as a promising solution to mitigate the shadowing, and dual-sided illumination[70,79] providing illumination from both sides of the sample, leads to improved imaging depth and better overall sample coverage. Multi-sided illumination, however, increases the overall complexity of the setup and requires precise synchronization of two opposing light sheets. Furthermore, as reported by Equations (2) and (3), resolution anisotropy usually affects image formation in the types of architectures with inhomogeneities along the longitudinal and the transversal direction. Possible solutions rely on the implementation of Bessel illuminations,[80] or as an alternative, on multiple-view imaging of a rotating sample,[81–83] even though it increases the photobleaching and requires long postprocessing phases to fuse the different acquisitions. Conversely, there exist also multi-view configurations that require no rotation of the sample, but instead, the implementation of multiple detection paths along orthogonal directions, leading to images with high resolution in all 3D.[84,85] The main limitation lies in the complexity of the setup and the need for advanced computational algorithms for image reconstruction. In 2011 Inverted light-sheet microscopy was proposed to solve the geometrical difficulties of specific samples.[86,87] The key feature of this technique is the use of an inverted microscope configuration, where the specimen is placed at the bottom of the imaging chamber (Figure 2c). In 2014, lattice light-sheet fluorescence microscopy (LLSFM), was introduced by Betzig et al. to illuminate the sample using a structured light sheet pattern,[88] typically generated using a spatial light modulator (SLM). Even with a slightly compromised penetration depth, LLSFM offers several benefits, including minimized background noise, enhanced imaging speed, and minimal phototoxicity. Notably, this approach allowed researchers to optically section thick samples with high and nearly isotropic 3D spatial resolution.[89] To overcome the issues due to the presence of two objectives, single objective-based systems (SO) have also been proposed.[90,91] SO shares an elegant optical scheme where the light sheet is inclined at an angle to the detection axis. However, the inclined light sheet introduces astigmatism, which needs to be corrected during image processing, increasing the computational burden.

Afterward, the main challenge with LSFM is determining whether it is the best method to image the target sample. **Table 1** summarizes the advantages and disadvantages of the main light-sheet designs mentioned above. Besides common benefits, the technical aspects of designs that prioritize user friendliness and practicality are still being refined today with significant efforts. Nowadays, there are readily available commercial configurations that aim to increase the LSFM's adaptability. One of the earliest products available was the light sheet Z.1 from Carl Zeiss Microscopy, a traditional SPIM that drew inspiration from the cornerstones of Huisken[57] and Stelzer.[79] Today, Zeiss's Light-sheet and Lattice Lightsheet, make LSFM suited for large optically cleared specimens and live cell imaging, respectively, at subcellular resolution. Alternatively, for high-resolution imaging of large, cleared tissues, LaVision BioTec's ultramicroscope, inspired by Dodt,[70] combines a very wide field of view and uniform light-sheet thickness. In addition to those, Applied Scientific Instrumentation provides parts for an inverted microscope with a single- or dual-sided light-sheet arrangement. The proposed design, ideated from Shroff's work,[85] is especially well suited for high-throughput screening of tissue culture cells and other samples that are typically prepared on glass coverslips.

 

**Table 1.** Comparative table of the main light-sheet configurations. The optical architecture, the main advantages and disadvantages, and example references are reported for each technique.

| LSFM architecture | Main optical characteristic | Main Advantages | Main disadvantages | References |
|---|---|---|---|---|
| Single side illumination | Illumination from one single side | – Low photodamage;<br>– Fast acquisition | – Shadowing;<br>– Limited depth of field;<br>– FOV inhomogeneities | Huisken et al.[57] |
| Multidirectional illumination | Simultaneous tilted light sheet or fast pivoting | – Reduced shadowing;<br>– Improved image quality | – Geometrical constraints;<br>– Increased photobleaching | Huisken and Steinier[81] |
| Dual-side illumination | Illumination from two sides (simultaneous or alternated) | – FOV homogeneity | – Complex design;<br>– Synchronization of pivoting | Dodt et al.[70] |
| Multiple-view imaging | Image recording from different views | – Isotropic resolution imaging;<br>– Improved 3D imaging | – Increased acquisition time;<br>– Increased photobleaching;<br>– Long postprocessing | Krzic et al.[83] |
| Lattice light-sheet | Uniform nondiffracting light sheet illumination | – Isotropic resolution | – Limited penetration deep for scattering samples | Chen et al.[86] |
| Inverted light-sheet | Optimized orientation of the illumination and detection objectives | – Compatible with common confocal and widefield sample mounting;<br>– Suitable for sliced samples | – Geometrical constraints due to objectives steric hindrance | Wu et al.[87] |
| Single objective light-sheet | Single objective for illumination and detection | – Reduction of sample geometrical constraints | – Limited FOV;<br>– Extensive optics for image realignment | Dunsby et al.[91] |

Instead, a possible option for a multiview design is provided by Bruker's MuVi. Notably, Leica Microsystems provides a confocal-plus-digital light-sheet combined solution, making a single system adaptable and able to meet various experimental needs.

Nevertheless, commercial systems can be expensive and might not exactly meet the researcher's needs. In this regard, the OpenSPIM platform was developed to offer a maximally cost-effective solution that enables anyone to build an entry-level system and further modify it for specific imaging needs.[92] Formalized as a do-it-yourself process, the platform has a highly active online community where very detailed instructions can be found for basic assembly and operations.

### 3.3. Sample Mounting for ExLSFM

The success of LSFM also greatly depends on the proper preparation and mounting of 3D samples to ensure optimal imaging results. Samples need to be embedded or mounted in a way that preserves their natural structures and minimizes light scattering and striping effects.[77] Also, implementing hydrogel blocking measures during image acquisition is essential for preventing any drift in the acquired images. For these reasons, sample mounting is a critical aspect of light-sheet microscopy, as it directly impacts image quality, sample stability, and the preservation of biological integrity. The mounting of expanded samples for ExLSFM strictly adheres to the conventional method employed for mounting samples in light-sheet imaging. Hydrogel embedding is a common and straightforward method. Samples are embedded in a hydrogel such as low-melting-point agarose, which provides support and immobilizes the specimen during imaging (Figure 2d). This technique is versatile and well-suited for a wide range of sample types, including tissues, organoids, and small model organisms. This method has been used for expanded samples by Glaser et al.[93] by employing agarose. Expanded hydrogel samples are trimmed and housed in a custom anodized chamber. This chamber is submerged in a 0.05× saline sodium citrate (SSC) solution, ensuring the hydrogel aligns with light paths. After removal, a warm 2% agarose solution in 0.05× SSC is poured behind the hydrogel for stability and left to solidify. The chamber is then sealed and left in 0.05× SSC overnight before imaging. However, the diffusion of agarose can affect the refractive index and induce scattering artifacts, potentially limiting imaging depth and quality. Another approach is based on the development of transparent sample chambers filled with liquid matching the appropriate refractive index, in which samples are suspended or embedded. These chambers, often composed of specialized materials with refractive indices closely matching that of the sample, significantly reduce refractive aberrations.[94,95] Certain works have utilized fluoropolymers, such as Teflon. Both fluorinated ethylene–propylene (FEP) and polytetrafluoroethylene (PTFE) have refractive indices ($n$ = 1.34) that are compatible with expanded hydrogel specimens.[96] These fluoropolymers can be fashioned into thin sheets, which can be tightly stretched to create drumhead-like surfaces. Such surfaces serve as optimal holders for expanded specimens, minimizing potential damage and immobilizing the sample during imaging. Utilizing this approach, Scardigli et al.[43] and Glaser et al.[96] successfully imaged a 4× expanded human brain cortex and mouse kidney section, respectively, without causing harm to the expanded gel. A similar approach is used by MESOSPIM that introduces a cuvette-based approach enabling imaging of large samples where samples are immersed in a solution/gel inside a glass cuvette.

In a microscope where specimens are suspended from above, such as commercial LSFM Zeiss Z.1 and MUVI, it can be advisable to use either the (super)glue or poly-lysine method

 

(Figure 2e). Initially, specimens can be secured to a coverslip or another thin, durable backing with these adhesives. The coverslip can subsequently be attached to the top-mounted sample rod. In certain setups, a 3D-printed adapter is utilized to mechanically connect to the sample rod. The gel-coated coverslip is then affixed to this adapter using (super)glue. As an example, Mascheroni et al.[97] demonstrated a method in which a slender gel strip was trimmed and affixed to a 24 × 50 mm glass slide with superglue. This approach ensured that the cells were oriented upward and not in direct contact with the adhesive, effectively addressing potential issues of gel movement or drift. This approach is well-suited for expanded cells but can have limits for large tissues or organs. On the other hand, flat mounting options, exemplified by systems like commercial SMARTSPIM and LaVision, offer a stable and controlled environment. In the same line, glass bottom dishes, as seen in the Zeiss LLS7 system, provide a convenient platform for imaging expanded adherent cells. Occasionally, specimens are affixed using hooks or pressed onto a pointed mounting plate (Figure 2f) yet these approaches unavoidably result in sample damage. When using an inverted LSFM setup, the sample can be directly placed onto a glass microscope slide or sandwiched between two coverslips[41] (Figure 2g). The sample can be held in place using adhesive or a specialized sample holder that fits over the slide. For instance, Wang et al.[98] affixed expanded samples onto a custom-made plastic holder using a Poly-L-Lysine coated 8 mm glass coverslip and adhesive. Finally, while not yet utilized for LSFM, bicomponent glues could serve as a viable alternative to secure the boundary gel, ensuring its stability across multiple acquisitions.[11] The choice of sample mounting method depends on the nature of the specimen and the desired imaging outcome, highlighting the need for a tailored approach to expanding the capabilities of ExM and ExLSFM.

## 4. Nanoscale Investigation of Biological Specimens Using ExLSFM

While innovative developments of LSFM and ExM have significantly advanced imaging capabilities, a novel strategy involves their combination into a single imaging procedure. The combined use of LSFM and ExM has facilitated research into a diverse range of biological fields, spanning from cell cultures to primate brain applications. Different ExM protocols and optical LSFM setups have been fine-tuned to align with the characteristics of expanded samples and their respective staining methods. For instance, Mascheroni et al.[97] utilized a commercial inverted SPIM to visualize expanded LAIV-infected A549 cells (**Table 2**). Utilizing an inverted LSFM allowed for a comprehensive scan of the entire specimen, resulting in 3D renderings of the fully infected cells. This method yielded superior image quality relative to other techniques examined, including confocal and widefield microscopy. Thus, ExLSFM emerges as a premier method for the detailed examination of the interplay between viral proteins and cellular organelles in intact cells. Additionally, ExLSFM has emerged as a compelling technique for comparative anatomical investigations, particularly in the Drosophila brain. As demonstrated by Boyden, Betzig, and colleagues,[99] the integration of a canonical ≈4× ExM with LLSFM enables comprehensive reconstruction of its entire brain, achieving ≈60 × 60 × 90 $nm^3$ of optical resolution (**Figure 3a**). This approach facilitated detailed examination of long-range tracing and stereotypy of neuron bundles (Figure 3b), and presynaptic densities at dopaminergic neurons across all regions of the fly brain. Furthermore, Lillvis et al.[100] present an innovative pipeline tailored for rapid imaging and reconstruction of synaptic connections in the fruit fly. This pipeline exploits a variant of ProExM, which achieves an eight-fold expansion and is combined with LLSFM. This combination aims to correlate the analysis of circuit structure with function and behavior within the same specimen. Shifting the focus beyond insect models, ExLSFM has been utilized to capture nanoscale volumetric images of songbird brains in zebra finches[101] and specific subregions in the mouse hippocampal DG and CA1 regions[102] (Figure 3c). Based on this data, a custom-made LSFM setup was used to conduct a nanoscale study of MAP-processed mouse brains and tumor xenotransplantation, stained with hematoxylin and eosin.[103] In this research, tumor fibrotic tissue underwent high-temperature denaturation, expanded four-fold, and was imaged with an effective optical resolution of ≈250 nm. This innovative combination of hematoxylin and eosin staining with nanoscale tumor sample reconstruction offers promising avenues for both research and clinical labs. ZOOM- and TREx-processed mouse brain samples were also successfully combined to custom LSFM to image neurons expressing Thy1-eYFP[20] and immunostained for Bassoon (a marker for excitatory and inhibitory presynaptic active zones) and Homer[33] (a marker for the excitatory postsynaptic apparatus). Applications of ExLSFM have been successfully demonstrated in primate samples. Glaser and colleagues introduced ExA-SPIM,[93] an innovative system capable of imaging a volume of 200 × 52 × 35 $mm^3$, with an effective optical resolution of 300 nm laterally and 800 nm axially for three-fold expanded tissues. This capability was employed to reconstruct both the macaque motor cortex and sections of the human visual cortex. Furthermore, human kidney sections[99] and paraffin-fixed slices of the human cortex[43] underwent expansion using ExPath and ProExM, respectively, and were then captured with designated LSFM systems (Figure 3d,e). Finally, by utilizing commercially available LSFM to visualize multiple transcripts in Thy1-YFP mouse brain slices with ExFISH, Boyden, and colleagues bridged the gap between protein and transcript visualization with nanoscale resolution.[25] Also, Wang et al.[98] introduced a significant enhancement for transcriptome visualization in thick brain sections (300 mm), emphasizing the 3D relationships among various cell types within brain structures. Their innovative approach, termed Expansion-Assisted Iterative-FISH (EASI–FISH), employs multi-round multiplexed RNA-FISH combined using commercial LSFM (Zeiss Lightsheet Z.1 microscope, Zeiss). EASI–FISH not only enables precise, in situ measurement of gene expression at the cellular level but is also tailored for efficient multi-round, multiplex FISH analysis across complete tissue volumes. These approaches not only offer a more comprehensive view of cellular processes at the molecular level but also set a new benchmark for in-depth biological analysis. Studying both proteins and transcripts in large biological tissues concurrently has the potential to profoundly transform our understanding of intricate cellular dynamics, marking a pivotal step for future research endeavors.

 

**Table 2.** Comparative table of the main ExLSFM application. The table summarizes the organism model studied by LSFM, the expansion protocol, anchor molecule, homogenization method, expansion factor, staining procedure, and the publication's reference.

| Sample | LSFM | ExM protocol | Anchor molecule | Digestion | Expansion factor | Staining | References |
|---|---|---|---|---|---|---|---|
| Infected A549 cell | Commercial iSPIM | Chozinski protocol | GA | Enzymatic proteolysis | Four fold | Immunostaining | Mascheroni et al.[97] |
| Drosophila Whole brain/connectome reconstruction | Lattice light sheet | ProExM and variant | AcX | Enzymatic proteolysis | Four and eight folds | Immunostaining | Gao et al.[99]<br>Lillvis et al.[100] |
| Zebra finches brain | Commercial LSFM (Ultra Microscope II, LaVision Biotec GmbH, Germany)) | ProExM | AcX | Enzymatic proteolysis | Four fold | Immunostaining | Düring et al.[101] |
| Mouse brain | ✲ Custom-built setup based on a Nikon Eclipse Ti-U inverted microscope (Nikon, Düsseldorf, Germany);<br>° Custom-made;<br>S,ε Commercial setup<br>(x SmartSPIM, Lifecanvas Technologies, MA;<br>T,¥ Zeiss Z1 lightsheet microscope) | ✲ Chozinski protocol;<br>S ExFISH;<br>° MAP;<br>x SHIELD-MAP;<br>ε ZOOM;<br>T TREx<br>¥ EASI-FISH | ✲ MA-NHS;<br>S LabelX;<br>°,x,ε AA<br>T,x AcX<br>¥ MelphaX | ✲,S,¥ Enzymatic proteolysis;<br>°,x,ε,T Thermal-chaotropic denaturation | ✲,°,x Four fold;<br>S,¥ Three fold;<br>ε Six fold;<br>T Ten fold | ✲,T Immunostaining;<br>x,ε GFP;<br>S,¥ Single molecule FISH;<br>° Hematoxylin and eosin | ✲ Bürgers et al.[102]<br>**S** Chen et al.[25]<br>° Laurino et al.[103]<br>**x** Park et al.[27]<br>**T** Damstra et al.[33]<br>ε Park et al.[20]<br>¥ Wang et al.[98] |
| Mouse kidney | Multi-immersion open-top light-sheet (OTLS) | Chozinski protocol | MA-NHS | Enzymatic proteolysis | Four fold | Immunostaining | Glaser et al.[96] |
| Mouse tumor xenograft | Custom-made setup | MAP | AA | Thermal-chaotropic denaturation | Four fold | hematoxylin and eosin | Laurino et al.[103] |
| Macaque motor cortex (1 × 1 × 1.5 cm block) | ExA-SPIM | Modified version of proExM | AcX | Enzymatic proteolysis | Three fold | Cortico-spinal neurons expressing a fluorescent protein (tdTomato) | Glaser et al.[93] |
| Human Kidney | Lattice light sheet | ExPath | AcX | Enzymatic proteolysis | Four fold | Immunostaining | Gao et al.[99] |
| Paraffin-fixed human cortex (100-µm thick pre-expansion) | Custom-made setup | ProExM | AcX | Enzymatic proteolysis | Four fold | Immunostaining | Scardigli et al.[43] |
| Human visual cortex (100-µm thick pre-expansion) | ExA-SPIM | Modified version of proExM | AcX | Enzymatic proteolysis | Four fold | Immunostaining | Glaser et al.[93] |

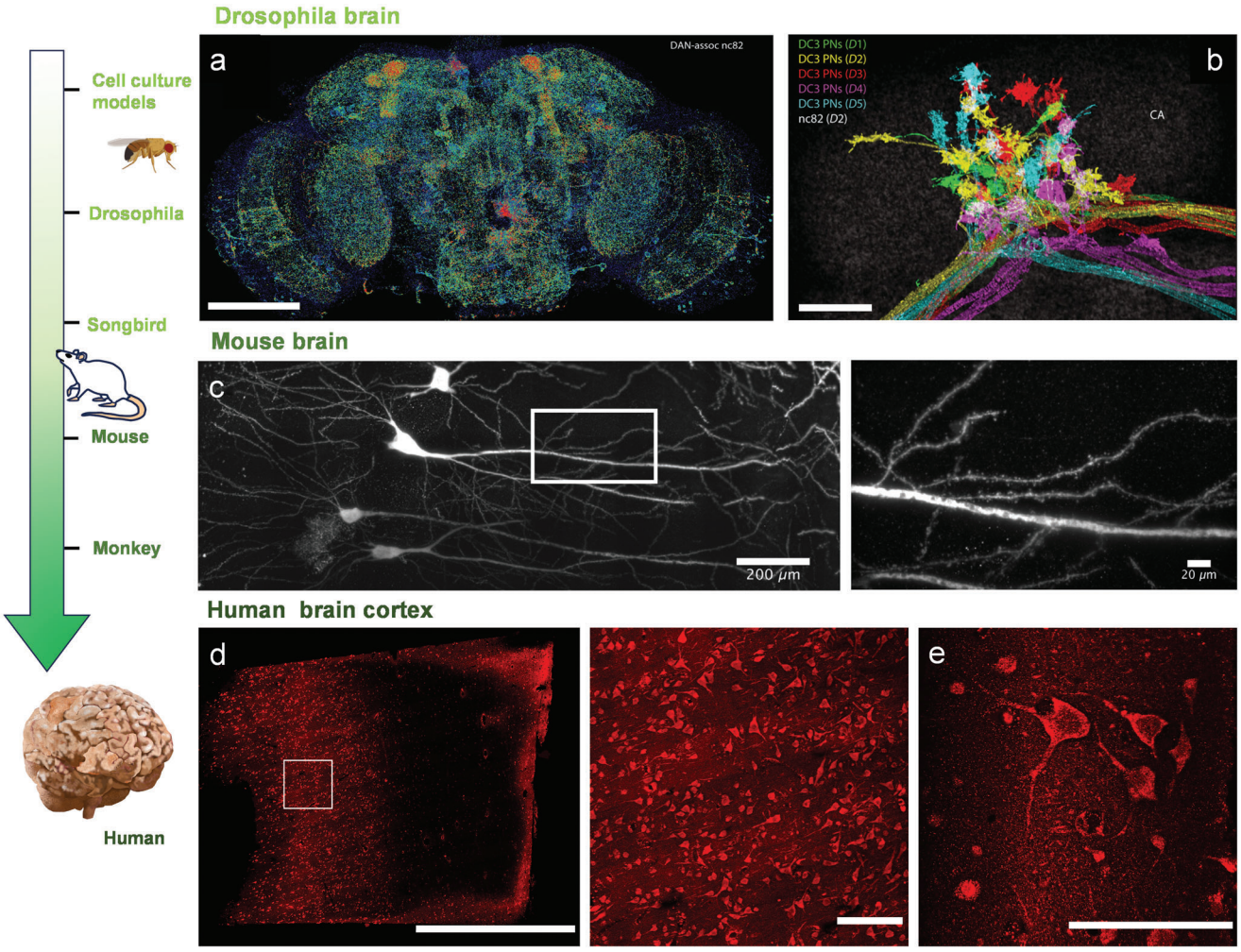


**Figure 3.** ExLSFM and its application across different organism models. a) Whole brain analysis of presynaptic sites and dopaminergic neurons in Drosophila, acquired using proExM and LLSFM. Scale bar: 100 μm. b) Overlaid maximum intensity projection view of DC3 olfactory projection neurons from five adult Drosophila brains (D1-D5) near CA. Scale bar: 10 μm. c) ExLSFM allows the identification of individual dendritic spines of sparsely labeled pyramidal neurons in CA1 in mice. d) Maximum intensity projection of postexpanded human superior frontal cortex and zoom-in of a specific region. The expanded brain slice (pre-expansion thick 100 um) was stained for NeuN and acquired using a custom-made LSFM. Downsampled reconstruction, scale bar 1 mm. e) High-resolution images of neurons labeled for the neuronal markers NeuN. Scale bar (400/4) = 100 um. Panels a, b, and c were adapted with permission from refs. [43,99,102].

## 5. Discussion and Conclusion

In this review, we provided insights into the present status of ExLSFM, emphasizing its core strengths and associated challenges as an integrated multi-modality. Indeed, the balance between image quality and 3D volume imaging poses a clear challenge for larger samples. When compared to traditional super-resolution microscopy techniques and sample-clearing processes, ExLSM offers a multitude of technical advantages. These encompass the ability to achieve 3D nanoscale imaging of multiple intricate biological structures within densely fixed samples while maintaining a swift and user-friendly application process. The main disadvantages of ExM in such an integrated approach lie in its limited compatibility with living samples and susceptibility to signal loss, posing challenges in real-time applications and dynamic studies involving living organisms.

The signal strength in expanded tissues is a highly delicate and crucial topic to address. Expansion enhances resolution but dilutes fluorescence intensity, e.g., a four-fold expansion reduces the signal by 64-fold. Pre-expansion treatments can also decrease fluorescence caused by enzymatic digestion and gel polymerization. To counteract signal loss, various amplification techniques, such as hybridization chain reaction and iterative antibody binding, have been introduced.[2,104,105] Also, traditional antibodies, especially when used with optically cleared tissue, find it hard to penetrate thicker samples. This leads to increased background noise due to sample volume and molecular crowding, in particular into the center of the specimen. Fortunately, recent advances in ExM can overcome this penetration barrier. Postexpansion labeling strategies, for instance, benefit from a "decrowding" effect, which increases fluorescence and reveals previously hidden nanostructures. Also, probe size is a critical factor in tissue

 

staining. While the resolution provided by ExM, based on advancements in gel chemistry, has not yet reached its theoretical peak, employing smaller labels can boost localization precision and guarantee consistent staining.

LSFM, a method gaining prominence over the last two decades, excels in deep imaging of expansive cleared tissues with minimal photobleaching and phototoxicity. This approach guarantees faster imaging speed compared with other nondestructive tomographic approaches such as magnetic resonance imaging and computerized tomography.[106] Following imaging, LSFM generates well-registered serial sections that can be used for additional histological procedures or 3D reconstructions.

Although these two technologies have been developed independently, in the last years numerous works demonstrated that their integration can lead to synergistic outcomes, enhancing the capabilities and performance of both in various applications. Several synergistic benefits arise from the combination of both techniques. Typically, the size of the specimen is not a limiting factor in many LSFM setups. For this reason, different expansion factors and multi-round approaches can be adopted. Specifically, ExLSFM enhances our ability to visualize nanoscale details in whole organs and tissues. Compared to other clearing techniques, the use of distilled water for Refractive Index (RI) matching is a safer and cost-effective alternative. Typically, LSFM demands a substantial amount of index-matching solution to diminish optical aberrations and enhance image contrast. The capability to employ water with expanded samples simplifies this procedure. Furthermore, LSFM offers a swift acquisition rate for expanded hydrogels. This minimizes exposure time and reduces the risk of the hydrogel drying out.

Tissue expansion works exceptionally well when combined with LSFM, allowing for the rapid generation of imaging data. As recommended by Schwarz and Kubitscheck,[107] ≈13 image tiles are needed to cover a 1 $mm^2$ object field when using a 40x objective lens with a numerical aperture of 1.0, while imaging at diffraction-limited resolution. Similarly, capturing optical sections spanning a 1 mm axial distance requires 3333 slices under optimal conditions, such as those needed for deconvolution. Consequently, imaging a specimen region with a volume of 1 $mm^3$ takes ≈30 min at a frame rate of 25 hertz.[107] This enables the rapid imaging of fluorescently sparsely labeled neurons, facilitating the creation of a super-resolved model of large brain areas and elucidating the long-range connections of brain nuclei. An additional example comes from the recent work of Glaser et al.[93] They developed ExA-SPIM, a refined version of LSFM tailored for expanded tissues, to exploit the synergic effect of ExM and LSFM. This system enables centimeter-scale tissue imaging with sub-micrometer resolutions at up to 1 gigaVoxel/sec.[93] This efficiency reduces the necessity for physical sectioning, streamlining imaging data, and simplifying subsequent analysis.

ExLSFM offers 3D nanoscale imaging across multiple colors, by preserving the integrity of protein profiles in entire organs and tissues. This ability permits multi-round labeling, crucial for visualizing various markers in intact tissues. The ability of ExM to optically clear and decrowd makes it instrumental for in-depth single-cell omics research, including proteomics and spatial transcriptomics. ExLSFM has the potential to redefine our approach to cellular and molecular biology. Their combined insights could significantly bolster our understanding of biology and associated diseases. Moreover, the potential applications of this method extend beyond pure research; it could also make a pivotal contribution to the clinical fields, paving the way for enhanced diagnosis.

## 6. Future Perspectives

ExLSFM has found applications in diverse fields such as neurobiology, virology, and nephrology. Given the customizability of ExLSFM, it presents an opportunity in solid tumor research, particularly for investigating the nanoscale intricacies of large biopsies. ExLSFM will deeply decipher the tumor's microenvironment, identify markers' activity, and track its biological progression over time. Enhanced by its high-throughput imaging capabilities, ExLSFM also holds promise for real-time intraoperative imaging and precise margin identification in conditions like squamous cell carcinoma.[108] Further, ExM has been pivotal in expanding cell nuclei to study chromatin ultrastructure. While protocols for nuclear imaging await standardization, the optimized method could revolutionize genetic and chromosomal studies in both clinical and preclinical settings. For example, ExLSFM will define the epigenetic modifications[109] in large tissue or biopsies, paving a new way for understanding several diseases, including cancer.

Given the complexity of cancer tissue structures and diverse biomolecule signatures, protocols like MAGNIFY,[26] which can simultaneously depict DNA, RNA, and proteins, or pan-ExM, designed for labeling the entire proteome,[110,111] are invaluable in deciphering these intricate assemblies. The robust structural integrity of these methods, coupled with the ability to stain a broad spectrum of biomolecules, makes them well-suited for advanced multiplexed imaging. Even though there are several clearing methods available for multi-marker studies using LSFM (in the human brain, for instance, seven different labels in the same sample),[41,112] the potential of ExLSFM in this domain remains largely unexplored.

The combination of ExM and LSFM addresses the challenges of subcellular resolution and imaging depth, providing a powerful toolset for researchers across diverse fields. In seeking deeper molecular understandings, it is essential to broaden our perspective and incorporate complementary techniques in a more comprehensive path from in vivo to cell investigation at different spatial resolutions and temporal scales. In this regard, the marriage of ExLSFM with positron emission tomography (PET) and autoradiography emerges as a potent strategy, enabling the concurrent visualization of molecular and structural details along with dynamic metabolic processes and seamlessly complementing the strengths of ExLSFM.

Positron Emission Tomography (PET),[113] is the hallmark molecular imaging method offering in vivo noninvasive insight into biological processes with molecular sensitivity. Exploiting radiolabeled probes, PET has established itself in the realm of cancer diagnosis and treatment. Considering that cancer often exhibits the intricate relationship between cancerous and noncancerous cells, the uptake heterogeneity and dynamics of Fludeoxyglucose F18 (18F-FDG) – a radioactive tracer that acts as a glucose analog – can provide a deeper understanding of tumor stage and aggressiveness. PET has excellent sensitivity but is limited by a low spatial resolution. Autoradiography,[114] can overcome the spatial resolution limitation of PET by offering

 

high-resolution spatial (50–100 micron) mapping of radiolabeled compounds ex vivo on thin slices of tissue, thus losing the dynamic information of PET.

These integrated approaches where the amalgamation of diverse techniques converge to provide a holistic understanding of cellular phenomena can benefit from the incorporation of ExLSFM with its capability to provide a detailed insight into the cellular microenvironment and molecular interactions that may drive the variability of tumor cell behavior, paving the way for new discoveries in cancer and other applications in biomedical research.

## Acknowledgements

GS received financial support from Unipa FFR 2023 and 2024. This work is partially supported by the NextGenerationEU Project PNRR-SEE LIFE – Strengthening the Italian Infrastructure of Euro-Bioimaging (IR23 – DD MUR 3264/21 CUPB53C22001810006).

## Conflict of interest

The authors declare no conflict of interest.

## Keywords

3D reconstruction, expansion microscopy, light-sheet fluorescence microscopy, multiplexed imaging, nanoscale imaging

Received: December 11, 2023
Revised: February 10, 2024
Published online: March 10, 2024

[1] A. Diaspro, P. Bianchini, F. Cella Zanacchi, L. Lanzanò, G. Vicidomini, M. Oneto, L. Pesce, I. Cainero, in *Springer Handbook of Microscopy* (Eds: P.W. Hawkes, J.C.H. Spence), Springer International Publishing, Cham **2019**, pp. 1039–1088.
[2] A. T. Wassie, Y. Zhao, E. S. Boyden, *Nat. Methods* **2019**, *16*, 33.
[3] G. Vicidomini, P. Bianchini, A. Diaspro, *Nat. Methods* **2018**, *15*, 173.
[4] K. Prakash, B. Diederich, R. Heintzmann, L. Schermelleh, *Philos. Trans. R. Soc. A Math. Phys. Eng. Sci.* **2022**, *380*, 20210110.
[5] M. Born, E. Wolf, *Principles of Optics: Electromagnetic Theory of Propagation, Interference and Diffraction of Light*, Elsevier, Amsterdam **2013**.
[6] H. R. Ueda, A. Ertürk, K. Chung, V. Gradinaru, A. Chédotal, P. Tomancak, P. J. Keller, *Nat. Rev. Neurosci.* **2020**, *21*, 61.
[7] F. Chen, P. W. Tillberg, E. S. Boyden, *Science* **2015**, *347*, 6221.
[8] R. Gräf, J. Rietdorf, T. Zimmermann, *Adv. Biochem. Eng. Biotechnol.* **2005**, *95*, 57.
[9] L. Pesce, M. Cozzolino, L. Lanzanò, A. Diaspro, P. Bianchini, *J. Biophotonics* **2019**, *12*, 201900018.
[10] M. Gao, R. Maraspini, O. Beutel, A. Zehtabian, B. Eickholt, A. Honigmann, H. Ewers, *ACS Nano* **2018**, *12*, 4178.
[11] P. Bianchini, L. Pesce, A. Diaspro, *Expansion Microscopy at the Nanoscale: The Nuclear Pore Complex as a Fiducial Landmark*, Elsevier Inc., Amsterdam **2021**.
[12] H. Xu, Z. Tong, Q. Ye, T. Sun, Z. Hong, L. Zhang, A. Bortnick, S. Cho, P. Beuzer, J. Axelrod, Q. Hu, M. Wang, S. M. Evans, C. Murre, L. F. Lu, S. Sun, K. D. Corbett, H. Cang, *Proc. Natl. Acad. Sci. USA* **2019**, *116*, 18423.
[13] F. U. Zwettler, S. Reinhard, D. Gambarotto, T. D. M. Bell, V. Hamel, P. Guichard, M. Sauer, *Nat. Commun.* **2020**, *11*, 3388.
[14] Y. Wang, Z. Yu, C. K. Cahoon, T. Parmely, N. Thomas, J. R. Unruh, B. D. Slaughter, R. S. Hawley, *Nat. Protoc.* **2018**, *13*, 1869.
[15] Y. Zhuang, X. Shi, *Curr. Opin. Struct. Biol.* **2023**, *81*, 102614.
[16] T. Ku, J. Swaney, J.-Y. Park, A. Albanese, E. Murray, J. H. Cho, Y.-G. Park, V. Mangena, J. Chen, K. Chung, *Nat. Biotechnol.* **2016**, *34*, 973.
[17] H. Singh, K. A. Bishen, D. Garg, H. Sukhija, D. Sharma, U. Tomar, *Dent. J. Adv. Stud.* **2019**, *07*, 051.
[18] D. French, J. T. Edsall, in Advances in Protein Chemistry, Academic Press, Cambridge **1945**.
[19] K. A. K. Tanaka, K. G. N. Suzuki, Y. M. Shirai, S. T. Shibutani, M. S. H. Miyahara, H. Tsuboi, M. Yahara, A. Yoshimura, S. Mayor, T. K. Fujiwara, A. Kusumi, *Nat. Methods* **2010**, *7*, 865.
[20] H. E. Park, D. Choi, J. S. Park, C. Sim, S. Park, S. Kang, H. Yim, M. Lee, J. Kim, J. Pac, K. Rhee, J. Lee, Y. Lee, Y. Lee, S. Y. Kim, *Adv. Sci.* **2019**, *6*, 1901673.
[21] K. N. Richter, N. H. Revelo, K. J. Seitz, M. S. Helm, D. Sarkar, R. S. Saleeb, E. D'Este, J. Eberle, E. Wagner, C. Vogl, D. F. Lazaro, F. Richter, J. Coy-Vergara, G. Coceano, E. S. Boyden, R. R. Duncan, S. W. Hell, M. A. Lauterbach, S. E. Lehnart, T. Moser, T. F. Outeiro, P. Rehling, B. Schwappach, I. Testa, B. Zapiec, S. O. Rizzoli, *EMBO J.* **2018**, *37*, 139.
[22] P. W. Tillberg, F. Chen, K. D. Piatkevich, Y. Zhao, C. C. Yu, B. P. English, L. Gao, A. Martorell, H. J. Suk, F. Yoshida, E. M. Degennaro, D. H. Roossien, G. Gong, U. Seneviratne, S. R. Tannenbaum, R. Desimone, D. Cai, E. S. Boyden, *Nat. Biotechnol.* **2016**, *34*, 987.
[23] J. Park, S. Khan, D. H. Yun, T. Ku, K. L. Villa, J. E. Lee, Q. Zhang, J. Park, G. Feng, E. Nedivi, K. Chung, *Sci. Adv.* **2021**, *7*, eabf6589.
[24] T. J. Chozinski, A. R. Halpern, H. Okawa, H. J. Kim, G. J. Tremel, R. O. L. Wong, J. C. Vaughan, *Nat. Methods* **2016**, *13*, 485.
[25] F. Chen, A. T. Wassie, A. J. Cote, A. Sinha, S. Alon, S. Asano, E. R. Daugharthy, J.-B. Chang, A. Marblestone, G. M. Church, A. Raj, E. S. Boyden, *Nat. Methods* **2016**, *13*, 679.
[26] A. Klimas, B. R. Gallagher, P. Wijesekara, S. Fekir, E. F. DiBernardo, Z. Cheng, D. B. Stolz, F. Cambi, S. C. Watkins, S. L. Brody, A. Horani, A. L. Barth, C. I. Moore, X. Ren, Y. Zhao, *Nat. Biotechnol.* **2023**, *41*, 858.
[27] Y. G. Park, C. H. Sohn, R. Chen, M. McCue, D. H. Yun, G. T. Drummond, T. Ku, N. B. Evans, H. C. Oak, W. Trieu, H. Choi, X. Jin, V. Lilascharoen, J. Wang, M. C. Truttmann, H. W. Qi, H. L. Ploegh, T. R. Golub, S. C. Chen, M. P. Frosch, H. J. Kulik, B. K. Lim, K. Chung, *Nat. Biotechnol.* **2019**, *37*, 73.
[28] S. Truckenbrodt, *Anal. Chem.* **2023**, *95*, 3.
[29] S. M. Asano, R. Gao, A. T. Wassie, P. W. Tillberg, F. Chen, E. S. Boyden, *Curr. Protoc. Cell Biol.* **2018**, *80*, e56.
[30] K. Chung, J. Wallace, S. Y. Kim, S. Kalyanasundaram, A. S. Andalman, T. J. Davidson, J. J. Mirzabekov, K. A. Zalocusky, J. Mattis, A. K. Denisin, S. Pak, H. Bernstein, C. Ramakrishnan, L. Grosenick, V. Gradinaru, K. Deisseroth, *Nature* **2013**, *497*, 332.
[31] S. Truckenbrodt, M. Maidorn, D. Crzan, H. Wildhagen, S. Kabatas, S. O. Rizzoli, *EMBO Rep.* **2018**, *19*, e45836.
[32] S. Truckenbrodt, C. Sommer, S. O. Rizzoli, J. G. Danzl, *Nat. Protoc.* **2019**, *14*, 832.
[33] H. G. J. Damstra, B. Mohar, M. Eddison, A. Akhmanova, L. C. Kapitein, P. W. Tillberg, *Elife* **2022**, *11*, 73775.
[34] X. Shi, Q. Li, Z. Dai, A. A. Tran, S. Feng, A. D. Ramirez, Z. Lin, X. Wang, T. T. Chow, J. Chen, D. Kumar, A. R. McColloch, J. F. Reiter, E. J. Huang, I. B. Seiple, B. Huang, *J. Cell Biol.* **2021**, *220*, 202105067.
[35] G. Wen, V. Leen, Y. Jia, T. Rohand, J. Hofkens, *Chem. – A Eur. J.* **2022**, *28*, 202202404.
[36] E. F. Fornasiero, F. Opazo, *BioEssays* **2015**, *37*, 436.
[37] H. Lee, C.-C. Yu, E. S. Boyden, X. Zhuang, P. Kosuri, *Sci. Rep.* **2021**, *11*, 16944.

 

[38] I. CHO, J. Y. SEO, J. CHANG, *J. Microsc.* **2018**, *271*, 123.
[39] D. Gambarotto, F. U. Zwettler, M. Le Guennec, M. Schmidt-Cernohorska, D. Fortun, S. Borgers, J. Heine, J. G. Schloetel, M. Reuss, M. Unser, E. S. Boyden, M. Sauer, V. Hamel, P. Guichard, *Nat. Methods* **2019**, *16*, 71.
[40] M. H. Laporte, N. Klena, V. Hamel, P. Guichard, *Nat. Methods* **2022**, *19*, 216.
[41] L. Pesce, M. Scardigli, V. Gavryusev, A. Laurino, G. Sancataldo, L. Silvestri, C. Destrieux, R. Patrick, I. Costantini, F. S. Pavone, **2021**.
[42] Y. Zhao, O. Bucur, H. Irshad, F. Chen, A. Weins, A. L. Stancu, E. Y. Oh, M. Distasio, V. Torous, B. Glass, I. E. Stillman, S. J. Schnitt, A. H. Beck, E. S. Boyden, *Nat. Biotechnol.* **2017**, *35*, 757.
[43] M. Scardigli, L. Pesce, N. Brady, G. Mazzamuto, V. Gavryusev, L. Silvestri, P. R. Hof, C. Destrieux, I. Costantini, F. S. Pavone, *Front. Neuroanat.* **2021**, *15*, 1.
[44] S. J. Edwards, V. Carannante, K. Kuhnigk, H. Ring, T. Tararuk, F. Hallböök, H. Blom, B. Önfelt, H. Brismar, *Front. Mol. Biosci.* **2020**, *7*, 1.
[45] R. Gao, C.-C. (Jay) Yu, L. Gao, K. D. Piatkevich, R. L. Neve, J. B. Munro, S. Upadhyayula, E. S. Boyden, *Nat. Nanotechnol.* **2021**, *16*, 698.
[46] C. Mao, M. Y. Lee, J. R. Jhan, A. R. Halpern, M. A. Woodworth, A. K. Glaser, T. J. Chozinski, L. Shin, J. W. Pippin, S. J. Shankland, J. T. C. Liu, J. T. C. Liu, J. T. C. Liu, J. C. Vaughan, J. C. Vaughan, *Sci. Adv.* **2020**, *6*, 22.
[47] K. A. Saal, A. H. Shaib, N. Mougios, D. Crzan, F. Opazo, S. O. Rizzoli, *Sci. Rep.* **2023**, *13*, 5366.
[48] J. Sim, C. E. Park, I. Cho, K. Min, J.-S. Lee, Y. Chong, J. Kim, J. S. Kang, K. D. Piatkevich, E. E. Jung, S.-K. Kwon, Y.-G. Yoon, E. S. Boyden, J.-B. Chang, *bioRxiv*, https://doi.org/10.1101/2021.05.18.443629, 2021.
[49] J.-B. Chang, F. Chen, Y.-G. Yoon, E. E. Jung, H. Babcock, J. S. Kang, S. Asano, H.-J. Suk, N. Pak, P. W. Tillberg, A. T. Wassie, D. Cai, E. S. Boyden, *Nat. Methods* **2017**, *14*, 593.
[50] R. Gao, S. M. Asano, E. S. Boyden, *BMC Biol.* **2017**, *15*, 50.
[51] R. S. Seehra, S. J. Warrington, B. H. K. Allouis, T. M. D. Sheard, M. E. Spencer, T. Shakespeare, A. Cadby, D. Bose, D. Strutt, I. Jayasinghe, *Cell Rep. Phys. Sci.* **2023**, 101719.
[52] L. A. Pugliese, V. De Lorenzi, M. Bernardi, S. Ghignoli, M. Tesi, P. Marchetti, L. Pesce, F. Cardarelli, *Sci. Rep.* **2023**, *13*, 13342.
[53] H. Deschout, F. C. Zanacchi, M. Mlodzianoski, A. Diaspro, J. Bewersdorf, S. T. Hess, K. Braeckmans, *Nat. Methods* **2014**, *11*, 253.
[54] C. J. Engelbrecht, E. H. Stelzer, *Opt. Lett.* **2006**, *31*, 1477.
[55] H. Siedentopf, R. Zsigmondy, *Ann. Phys.* **1902**, *315*, 1.
[56] A. H. Voie, D. H. Burns, F. A. Spelman, *J. Microsc.* **1993**, *170*, 229.
[57] J. Huisken, J. Swoger, F. Del Bene, J. Wittbrodt, E. H. K. Stelzer, *Science* **2004**, *305*, 1007.
[58] K. Chatterjee, F. W. Pratiwi, F. C. M. Wu, P. Chen, B.-C. Chen, *Appl. Spectrosc.* **2018**, *72*, 1137.
[59] M. Weber, J. Huisken, *Curr. Opin. Genet. Dev.* **2011**, *21*, 566.
[60] G. de Vito, L. Turrini, C. Müllenbroich, P. Ricci, G. Sancataldo, G. Mazzamuto, N. Tiso, L. Sacconi, D. Fanelli, L. Silvestri, F. Vanzi, F. S. Pavone, *Biomed. Opt. Express* **2022**, *13*, 1516.
[61] X. Chen, Y. Mu, Y. Hu, A. T. Kuan, M. Nikitchenko, O. Randlett, A. B. Chen, J. P. Gavornik, H. Sompolinsky, F. Engert, M. B. Ahrens, *Neuron* **2018**, *100*, 876.
[62] W. C. Lemon, S. R. Pulver, B. Höckendorf, K. McDole, K. Branson, J. Freeman, P. J. Keller, *Nat. Commun.* **2015**, *6*, 7924.
[63] J. van Krugten, K.-K. H. Taris, E. J. G. Peterman, *J. Microsc.* **2021**, *281*, 214.
[64] P. J. Keller, A. D. Schmidt, J. Wittbrodt, E. H. K. Stelzer, *Science* **2008**, *322*, 1065.
[65] E. M. C. Hillman, V. Voleti, W. Li, H. Yu, *Annu. Rev. Neurosci.* **2019**, *42*, 295.
[66] F. Pampaloni, N. Ansari, P. Girard, E. H. K. Stelzer, in *Proc. 2011 Advanced Microscopy Technique II*, (Eds: P.T.C. So, E. Beaurepaire), Optica Publishing Group, Washington, DC **2011**, p. 80860Y.
[67] O. E. Olarte, J. Andilla, E. J. Gualda, P. Loza-Alvarez, *Adv. Opt. Photon.* **2018**, *10*, 111.
[68] H. Kafian, S. Mozaffari-Jovin, M. Bagheri, S. A. Mousavi Shaegh, *Phys. Scr.* **2023**, *98*, 082001.
[69] K. Keomanee-Dizon, M. Jones, P. Luu, S. E. Fraser, T. V Truong, *Appl. Phys. Lett.* **2022**, *121*, 163701.
[70] H.-U. Dodt, U. Leischner, A. Schierloh, N. Jährling, C. P. Mauch, K. Deininger, J. M. Deussing, M. Eder, W. Zieglgänsberger, K. Becker, *Nat. Methods* **2007**, *4*, 331.
[71] P. Ricci, G. Sancataldo, V. Gavryusev, A. Franceschini, M. C. Müllenbroich, L. Silvestri, F. S. Pavone, *Biomed. Opt. Express* **2020**, *11*, 3111.
[72] T. Vettenburg, H. I. C. Dalgarno, J. Nylk, C. Coll-Lladó, D. E. K. Ferrier, T. Čižmár, F. J. Gunn-Moore, K. Dholakia, *Nat. Methods* **2014**, *11*, 541.
[73] F. O. Fahrbach, A. Rohrbach, *Nat. Commun.* **2012**, *3*, 632.
[74] M. C. Müllenbroich, L. Turrini, L. Silvestri, T. Alterini, A. Gheisari, N. Tiso, F. Vanzi, L. Sacconi, F. S. Pavone, *Front. Cell. Neurosci.* **2018**, *12*, 315.
[75] L. Silvestri, A. Bria, L. Sacconi, G. Iannello, F. S. Pavone, *Opt. Express* **2012**, *20*, 20582.
[76] V. Gavryusev, G. Sancataldo, P. Ricci, A. Montalbano, C. Fornetto, L. Turrini, A. Laurino, L. Pesce, G. de Vito, N. Tiso, F. Vanzi, L. Silvestri, F. S. Pavone, *J. Biomed. Opt.* **2019**, *24*, 106504.
[77] P. Ricci, V. Gavryusev, C. Müllenbroich, L. Turrini, G. de Vito, L. Silvestri, G. Sancataldo, F. S. Pavone, *Prog. Biophys. Mol. Biol.* **2021**, *168*, 52.
[78] G. Sancataldo, V. Gavryusev, G. de Vito, L. Turrini, M. Locatelli, C. Fornetto, N. Tiso, F. Vanzi, L. Silvestri, F. S. Pavone, *Front. Neuroanat.* **2019**, *13*, 1.
[79] J. Huisken, D. Y. R. Stainier, *Opt. Lett.* **2007**, *32*, 2608.
[80] T. A. Planchon, L. Gao, D. E. Milkie, M. W. Davidson, J. A. Galbraith, C. G. Galbraith, E. Betzig, *Nat. Methods* **2011**, *8*, 417.
[81] J. Swoger, P. Verveer, K. Greger, J. Huisken, E. H. K. Stelzer, *Opt. Express* **2007**, *15*, 8029.
[82] J. Nie, S. Liu, T. Yu, Y. Li, J. Ping, P. Wan, F. Zhao, Y. Huang, W. Mei, S. Zeng, D. Zhu, P. Fei, *Adv. Sci.* **2020**, *7*, 1901891.
[83] U. Krzic, S. Gunther, T. E. Saunders, S. J. Streichan, L. Hufnagel, *Nat. Methods* **2012**, *9*, 730.
[84] R. K. Chhetri, F. Amat, Y. Wan, B. Höckendorf, W. C. Lemon, P. J. Keller, *Nat. Methods* **2015**, *12*, 1171.
[85] Y. Wu, P. Wawrzusin, J. Senseney, R. S. Fischer, R. Christensen, A. Santella, A. G. York, P. W. Winter, C. M. Waterman, Z. Bao, D. A. Colón-Ramos, M. McAuliffe, H. Shroff, *Nat. Biotechnol.* **2013**, *31*, 1032.
[86] P. Strnad, S. Gunther, J. Reichmann, U. Krzic, B. Balazs, G. de Medeiros, N. Norlin, T. Hiiragi, L. Hufnagel, J. Ellenberg, *Nat. Methods* **2016**, *13*, 139.
[87] Y. Wu, A. Ghitani, R. Christensen, A. Santella, Z. Du, G. Rondeau, Z. Bao, D. Colón-Ramos, H. Shroff, *Proc. Natl. Acad. Sci* **2011**, *108*, 17708.
[88] B.-C. Chen, W. R. Legant, K. Wang, L. Shao, D. E. Milkie, M. W. Davidson, C. Janetopoulos, X. S. Wu, J. A. Hammer 3rd, Z. Liu, B. P. English, Y. Mimori-Kiyosue, D. P. Romero, A. T. Ritter, J. Lippincott-Schwartz, L. Fritz-Laylin, R. D. Mullins, D. M. Mitchell, J. N. Bembenek, A.-C. Reymann, R. Böhme, S. W. Grill, J. T. Wang, G. Seydoux, U. S. Tulu, D. P. Kiehart, E. Betzig, *Science* **2014**, *346*, 1257998.
[89] C. Zhang, Y. Chen, W. Liu, C. Kuang, Z. Zhang, X. Hao, X. Liu, *Opt. Lett.* **2020**, *45*, 2854.
[90] R. Strack, *Nat. Methods* **2021**, *18*, 28.

 

[91] C. Dunsby, *Opt. Express* **2008**, *16*, 20306.
[92] P. G. Pitrone, J. Schindelin, L. Stuyvenberg, S. Preibisch, M. Weber, K. W. Eliceiri, J. Huisken, P. Tomancak, *Nat. Methods* **2013**, *10*, 598.
[93] A. Glaser, J. Chandrashekar, J. Vasquez, C. Arshadi, N. Ouellette, X. Jiang, J. Baka, G. Kovacs, M. Woodard, S. Seshamani, K. Cao, N. Clack, A. Recknagel, A. Grim, P. Balaram, E. Turschak, A. Liddell, J. Rohde, A. Hellevik, K. Takasaki, L. E. Barner, M. Logsdon, C. Chronopoulos, S. de Vries, J. Ting, S. Perlmutter, B. Kalmbach, N. Dembrow, R. C. Reid, et al., *eLife* **2023**, https://doi.org/10.7554/elife.91979.1 RP91979.
[94] A. Kaufmann, M. Mickoleit, M. Weber, J. Huisken, *Development* **2012**, *139*, 3242.
[95] M. Weber, M. Mickoleit, J. Huisken, *J. Vis. Exp.* **2014**, *27*, e51119.
[96] A. K. Glaser, N. P. Reder, Y. Chen, C. Yin, L. Wei, S. Kang, L. A. Barner, W. Xie, E. F. McCarty, C. Mao, A. R. Halpern, C. R. Stoltzfus, J. S. Daniels, M. Y. Gerner, P. R. Nicovich, J. C. Vaughan, L. D. True, J. T. C. Liu, *Nat. Commun.* **2019**, *10*, 2781.
[97] L. Mascheroni, K. M. Scherer, J. D. Manton, E. Ward, O. Dibben, C. F. Kaminski, *Biomed. Opt. Express* **2020**, *11*, 5032.
[98] Y. Wang, M. Eddison, G. Fleishman, M. Weigert, S. Xu, T. Wang, K. Rokicki, C. Goina, F. E. Henry, A. L. Lemire, U. Schmidt, H. Yang, K. Svoboda, E. W. Myers, S. Saalfeld, W. Korff, S. M. Sternson, P. W. Tillberg, *Cell* **2021**, *184*, 6361.
[99] R. Gao, S. M. Asano, S. Upadhyayula, I. Pisarev, D. E. Milkie, T.-L. Liu, V. Singh, A. Graves, G. H. Huynh, Y. Zhao, J. Bogovic, J. Colonell, C. M. Ott, C. Zugates, S. Tappan, A. Rodriguez, K. R. Mosaliganti, S.-H. Sheu, H. A. Pasolli, S. Pang, C. S. Xu, S. G. Megason, H. Hess, J. Lippincott-Schwartz, A. Hantman, G. M. Rubin, T. Kirchhausen, S. Saalfeld, Y. Aso, E. S. Boyden, et al., *Science* **2019**, *363*, 6424.
[100] J. L. Lillvis, H. Otsuna, X. Ding, I. Pisarev, T. Kawase, J. Colonell, K. Rokicki, C. Goina, R. Gao, A. Hu, K. Wang, J. Bogovic, D. E. Milkie, L. Meienberg, B. Mensh, E. S. Boyden, S. Saalfeld, P. W. Tillberg, B. J. Dickson, *Elife* **2022**, *11*, 1.
[101] D. N. Düring, M. D. Rocha, F. Dittrich, M. Gahr, R. H. R. Hahnloser, *Front. Neuroanat.* **2019**, *13*, 1.
[102] J. Bürgers, I. Pavlova, J. E. Rodriguez-Gatica, C. Henneberger, M. Oeller, J. A. Ruland, J. P. Siebrasse, U. Kubitscheck, M. K. Schwarz, *Neurophotonics* **2019**, *6*, 1.
[103] A. Laurino, A. Franceschini, L. Pesce, L. Cinci, A. Montalbano, G. Mazzamuto, G. Sancataldo, G. Nesi, I. Costantini, L. Silvestri, F. S. Pavone, *Int. J. Mol. Sci.* **2023**, *24*, 6747.
[104] Y. Zhuo, B. Fu, R. Peng, C. Ma, S. Xie, L. Qiu, *Talanta* **2023**, *260*, 124541.
[105] Y. Cho, J. Seo, Y. Sim, J. Chung, C. E. Park, C. G. Park, D. Kim, J.-B. Chang, *Nanoscale* **2020**, *12*, 23506.
[106] P. A. Santi, *J. Histochem. Cytochem. Off. J. Histochem. Soc.* **2011**, *59*, 129.
[107] M. K. Schwarz, U. Kubitscheck, *Prog. Biophys. Mol. Biol.* **2022**, *168*, 33.
[108] S. Ghosh, B. S. Sapkota, R. S. Rao, S. Patil, C. Rajkumar, S. Lakshminarayan, *J. Microsc.* **2023**, *290*, 3.
[109] A. Acke, S. Van Belle, B. Louis, R. Vitale, S. Rocha, T. Voet, Z. Debyser, J. Hofkens, *Nucleic Acids Res.* **2022**, *50*, e100.
[110] O. M'Saad, J. Bewersdorf, *Nat. Commun.* **2020**, *11*, 1.
[111] O. M'Saad, R. Kasula, I. Kondratiuk, P. Kidd, H. Falahati, J. E. Gentile, R. F. Niescier, K. Watters, R. C. Sterner, S. Lee, X. Liu, P. De Camilli, J. E. Rothman, A. J. Koleske, J. Bewersdorf, *BioRxiv, Apr.* **2022**.
[112] E. Murray, J. H. Cho, D. Goodwin, T. Ku, J. Swaney, S. Y. Kim, H. Choi, Y. G. Park, J. Y. Park, A. Hubbert, M. McCue, S. Vassallo, N. Bakh, M. P. Frosch, V. J. Wedeen, H. S. Seung, K. Chung, *Cell* **2015**, *163*, 1500.
[113] A. Del Guerra, N. Belcari, M. Bisogni, *La Riv. del Nuovo Cim.* **2016**, *39*, 155.
[114] A. McEwen, C. Henson, *Bioanalysis* **2015**, *7*, 557.

 